Journal of Alloys and Compounds 509 (2011) 9970–9976

Contents lists available at ScienceDirect

Journal of Alloys and Compounds

journal homepage: www.elsevier.com/locate/jallcom

Characteristics of N-doped TiO_2 nanotube arrays by N_2-plasma for visible light-driven photocatalysis

Xu Liu, Zhongqing Liu*, Jian Zheng, Xin Yan, Dandan Li, Si Chen, Wei Chu*

College of Chemical Engineering, Sichuan University, Chengdu 610065, PR China

ARTICLE INFO

Article history:
Received 20 January 2011
Received in revised form 1 August 2011
Accepted 3 August 2011
Available online 10 August 2011

Keywords:
N_2-plasma
Titanium dioxide
Nanotube arrays
Visible-light activity

ABSTRACT

N-doped TiO_2 nanotube arrays were prepared by electrochemical anode oxidation of Ti foil followed by treatment with N_2-plasma and subsequent annealed under Ar atmosphere. The morphologies, composition and optical properties of N-doped TiO_2 nanotube arrays were characterized using field-emission scanning electron microscope (FE-SEM), transmission electron microscope (TEM), X-ray photoelectron spectroscopy (XPS), X-ray diffraction spectrometer (XRD), Photoluminescence (PL) and UV–vis diffusion reflection spectroscopy (UV–vis DRS). Methylene blue (MB) solution was utilized as the degradation model to evaluate the photocatalytic activity of the samples under visible light irradiation. The results suggested N_2-plasma treatment created doping of nitrogen onto the surface of photoelectrodes successfully and the N-doped TiO_2 nanotube arrays display a significantly enhancement of the photocatalytic activity comparing with the pure TiO_2 nanotube arrays under the visible light irradiation.

1. Introduction

Since the discovery of the phenomenon of photocatalytic splitting of water on TiO_2 electrode under ultraviolet light by Fujishima and Honda [1], TiO_2 has attracted much attention because of its possible application such as carrier of catalysts [2], pollutant degradation [3–6], gas sensor [7,8], photovoltaic cells [9–12] and photolysis of water [13–15]. However, a serious disadvantage of TiO_2 is its relatively large band gap between 3.0 eV (rutile) and 3.2 eV (anatase). Therefore, it can be excited only under ultraviolet irradiation, which merely accounts for about 5% of the solar radiation at the Earth's surface compared to the visible light occupying about 45%. To overcome this shortcoming of TiO_2, many attempts have been adopted to narrow the wide band gap of TiO_2 and suppress the recombination of photogenerated carries, such as doping with metal or non-metal ions [16–37], coupling with low band gap semiconductor [38,39], dye sensitization [40,41], surface modification and supporting noble metal [42,43].

Many previous studies demonstrated that doping TiO_2 with nitrogen was one of the most effective approaches to improve photocatalytic activity of TiO_2 in visible light regions [44,45]. For example, Asahi et al. reported that N-doped TiO_2 by sputtering the TiO_2 target in N_2 atmosphere showed photocatalytic activity for the decomposition of organic compound in wavelengths up to 550 nm [16], which attracted a great attention of N-doped TiO_2 as a visible light photocatalyst. Up to now, a variety of methods such as sputtering method [24,25], annealing under ammonia gas [26,27], ion implantation method [28,29], dip calcinations method [6,30], hydrothermal method [33], sol–gel method [34] and electrochemistry method [35] have been extensively carried out to dope nitrogen into TiO_2.

Although N-doped TiO_2 materials have been widely studied in literature during the past 10 years, most of previous works has been devoted to synthesis of N-doped TiO_2 powders or thin compact films and there are very few investigations related to N-doped TiO_2 nanotube arrays with visible light response. In this present work, we firstly fabricated a highly ordered TiO_2 nanotube arrays by anodization method. And then, the N-doped TiO_2 nanotube arrays were prepared through nitrogen plasma treatment. Nitrogen plasma is an effective and low cost technique to synthesize N-doping TiO_2 nanotube arrays, and avoid using the big expensive equipment, hazardous gas and organic compound. Photocatalytic activity of doped and undoped TiO_2 nanotube arrays was investigated, and the as-prepared novel materials excited excellent photocatalytic activity under visible light.

2. Experimental

2.1. Materials

Titanium sheets (0.5 mm thick, 20 mm × 30 mm size) with 99.6% purity were mechanically polished to a mirror image with no. 360 and 2000 silicon carbide abrasive paper successively. Following, they were chemically etched by soaking in a mixture of HF and HNO_3 ($HF:HNO_3:H_2O = 1:4:5$, v/v) for 20 s to eliminate the flaws resulting from polishing process. After that, the foils were rinsed with distilled water

* Corresponding authors.
E-mail addresses: 301zql@vip.sina.com (Z. Liu), chuwei1965_scu@yahoo.com, chuwei1965@scu.edu.cn (W. Chu).

0925-8388/$ – see front matter © 2011 Elsevier B.V. All rights reserved.
doi:10.1016/j.jallcom.2011.08.003

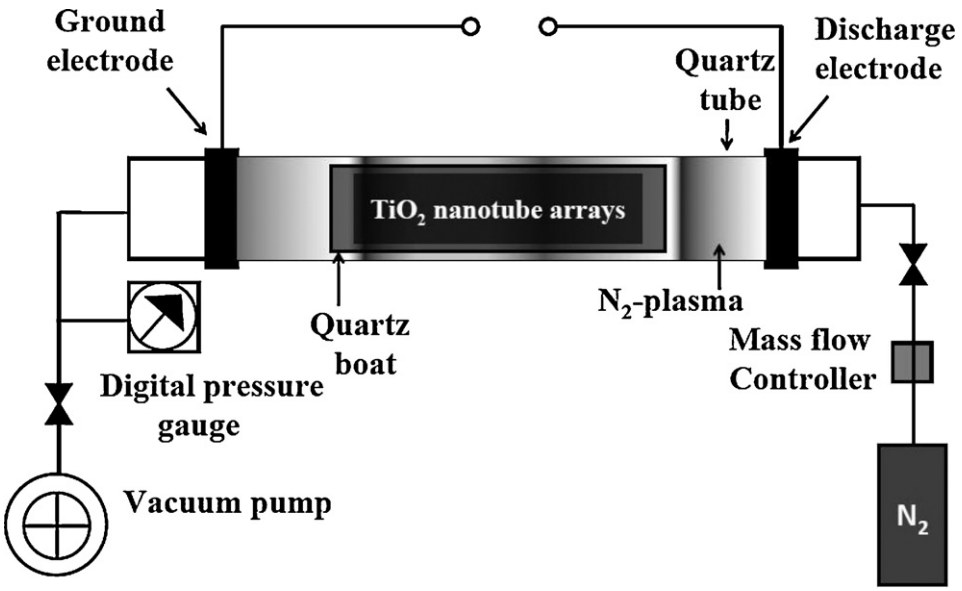

Fig. 1. Experimental for TiO_2 nanotube arrays treated with N_2-plasma.

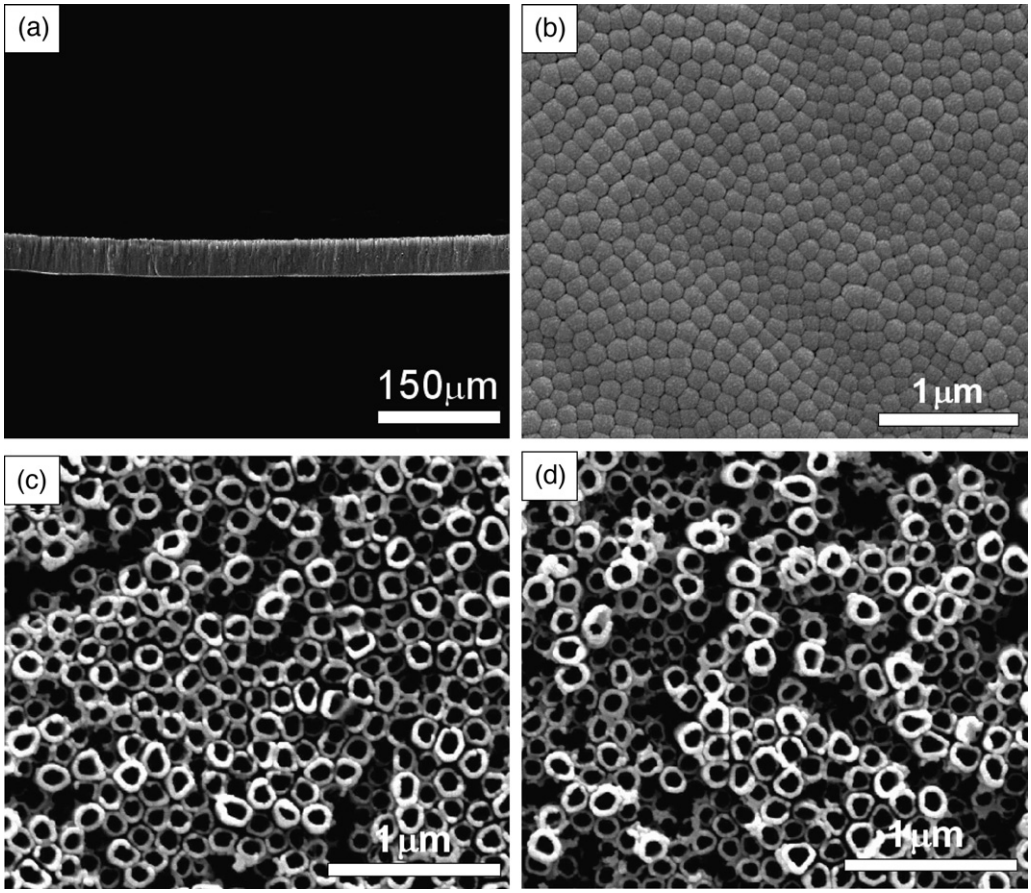

Fig. 2. (a) Cross-sectional and (b) bottom view SEM images of TN, top-view SEM images of (c) TN and (d) NPTN.

and dried in ambient air. So far, a working electrode was obtained. The graphite electrode was high-purity grade. Chemical reagents were all analytical reagent grade quality and used as received.

2.2. Preparation of TiO_2 nanotube arrays

The highly ordered and well-aligned TiO_2 nanotube arrays were prepared by anodization of Ti sheets in a conventional two-electrode configuration at a constant potential of 50 V at room temperature for 4 h, with high-purity graphite as the counter electrode. The distance between two electrodes was fixed at 8 cm in all experiments. To obtain TiO_2 nanotube arrays, titanium sheets were anodized in a glycerol system with 0.2 wt.% HF, 0.5 wt.% NH_4F and 2 vol.% H_2O. After anodization, the samples were rinsed by distilled water, and then air-dried. The as-prepared TiO_2 nanotube arrays were directly annealed at 500 °C for 2 h in air atmosphere, which were denoted as TN; or annealed at 500 °C for 2 h in Ar gas after being modified with N_2-plasma for 30 min, namely NPTN.

2.3. Plasma treatment

Fig. 1 shows a schematic of the experimental set-up for as-prepared TiO_2 nanotube arrays treated with N_2 plasma. The reactor consists of a 2.2 cm inner diameter quartz tube and two copper electrodes attached to the outer surface of the quartz tube. The distance between the electrodes was set at the electrode gap of 10 cm. Glow plasma was generated between the electrodes by using a home-built RF power. The reactor was operated at a pressure of 200 Pa with a mass flow controller where N_2 gas was dispersed into the reactor from the discharge electrode towards the ground electrode. The as-prepared TiO_2 nanotube arrays set in a quartz boat were placed inside the plasma reactor between the copper electrodes.

2.4. Characterization techniques

The morphology of the samples was observed using FE-SEM (FEI Corporation) and TEM (Tecnai G2 F20 S-Twin). The crystal structure of the obtained products was examined by XRD using a Philip X'Pert PRO diffractometer equipped with Cu Kα radiation in the 2θ range 20–80°, employing a step size of 0.03°. The accelerating voltage was set at 40 kV with 40 mA flux. XPS were performed with a Kratos XSAM-800 spectrometer using Al Kα (1486.6 eV) X-ray source at 12 kV and 15 mA, and the analytical instrument was corrected by standard samples of Au and Ag. All the binding energies were referenced to the C1s peak at 284.8 eV of the surface adventitious carbon. UV–vis DRS were conducted at room temperature on a PERSEE TU-1901 spectrophotometer. PL measurements were conducted at room temperature on an F-7000 FL spectrophotometer using a 300 nm excitation light. A two-electrode configuration was used to measure the photocurrent response, in which a 350 W Xenon lamp was utilized as light source, a titanium-based TiO_2 nanotube arrays close to lamp light to receive light irradiation served as the working electrode, a high-purity graphite was used as the cathode, 0.05 M Na_2SO_4 aqueous solution was used as the electrolyte. The distance between the Xenon lamp and the working electrode was 10 cm.

2.5. Photocatalytic experiments

All catalytic experiments were conducted in a specially designed rectangular quartz cell, in which a 350 W Xe lamp with a $CuSO_4$ filter served as a light source. The distance between the two electrodes was set at 2 cm. Photocatalytic activity of the as prepared nanotube arrays were estimated by measuring the degradation rate of methylene blue (10 mg L^{-1}). The amounts of methylene blue (MB) that remained after photo irradiation were determined at 660 nm every 10 min by a Vis spectrophotometer.

3. Results and discussion

3.1. SEM analysis

Well-aligned, high aspect ratio TiO_2 nanotube arrays were grown on Ti foil by electrochemical anodic oxidation in glycerol-base electrolyte at 50 V for 4 h. The surface morphology of NPTN and TN characterized by FE-SEM is shown in Fig. 2(a–c) shows the FE-SEM images of the cross-sectional, bottom and top-view of TN, respectively. The average inside diameter of the nanotube is ~140 nm with the wall thickness is ~30 nm and the length of nanotube is ~42 μm corresponding to a high aspect ratio of ~210. The bottom of nanotubes is end-closed and presents a hexagonal structure (Fig. 2(b)) [38,46]. Fig. 2(d) also displays the top-view of NPTN. Compared with TN, no clear change in the morphology of NPTN can be observed, indicating that the ordered nanotube arrays structure can be sustained the impact of N_2-plasma treatment.

3.2. XPS analysis

The general scan spectrum of XPS over a large energy range at low resolution was used to distinguish the elements present in the surface of PNTN and TN. The sharp peaks for Ti, O, and C elements were detected in both PNTN and TN, but no nitrogen signal was detected in TN (see Fig. 3(a)) while a weak nitrogen peak presented in NPTN (see Fig. 3(b)). The insets of Fig. 3 are N1s core level of the corresponding XPS spectra at higher resolution. The single N1s peak at the binding energy of 399.6 eV was detected in NPTN and the content of N element is approximately 2 at.%. Generally, the N1s centered at typical binding energy of around 396 eV is usually attributed to the formation of N–Ti–N structure, namely

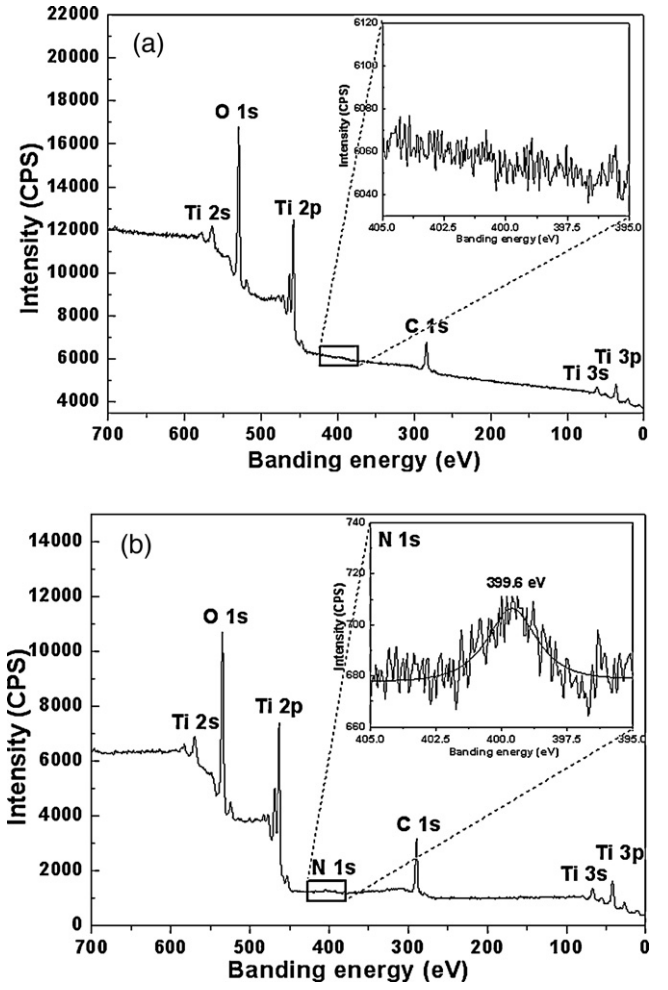

Fig. 3. XPS spectra of (a) TN and (b) NPTN. Inset is the enlarged range of the N1s peak.

substitutional N; meanwhile, the N1s peak at around 400 eV is ascribed to the N–Ti–O structure and above 400 eV is ascribed to Ti–N–O or NO_x species, mostly in interstitial N. The results were supported by the previous works on the N-doped TiO_2 nanoparticles and nanotubes [20,34]. We also noticed that the N1s band energy of around 400 eV was ascribed to chemisorbed N_2 in the N-doped nanoparticles prepared by ion implanting method [28,29]. But this state would not occur in our case, because the chemisorbed N_2 should be desorbed during the calcination at 500 °C under Ar atmospheres for 2 h. Thus, the N-doped samples obtained in our experiments should be assigned to interstitial N-doped TiO_2, which is accepted as a positive effect state in the photocatalytic reaction. This result proved that N-doped TiO_2 nanotube arrays can be prepared successfully via N_2-plasma treatment.

High-resolution N1s XPS spectra of the samples modified with N_2-plasma for different time is shown in Fig. S1. The XPS results confirmed that: (1) all the incorporated nitrogen was interstitial N-doped TiO_2; (2) the nitrogen concentrations of the samples modified with N_2-plasma for 60 min, 30 min and 10 min, subsequently annealed at 500 °C for 2 h in Ar atmosphere, were about 2.9, 2.0 and 0.6 at.%, respectively. Thus, the doped nitrogen concentration in modified TiO_2 nanotube arrays is related to the N_2-plasma treatment time. However, when the samples treated with N_2-plasma were annealed at 500 °C in an oxygen atmosphere, nitrogen could be generally removed as the generation of NO_x (shown in Fig. S2). While, doped nitrogen are retained within the nanotubes when annealing in a tube furnace with oxygen-free atmosphere. Hence,

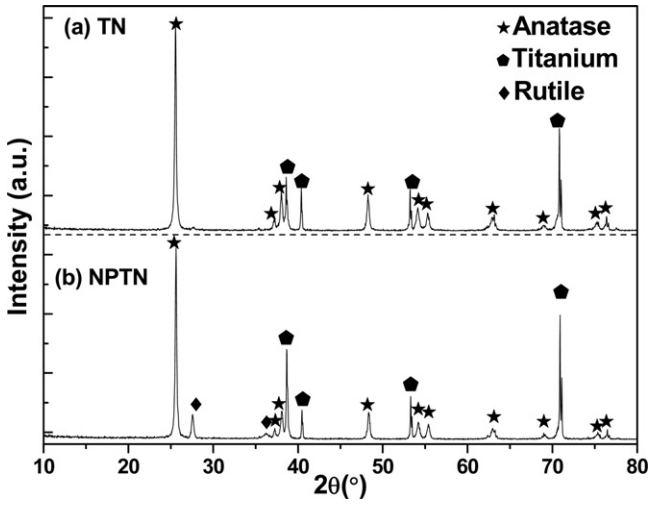

Fig. 4. XRD patterns of (a) TN and (b) NPTN.

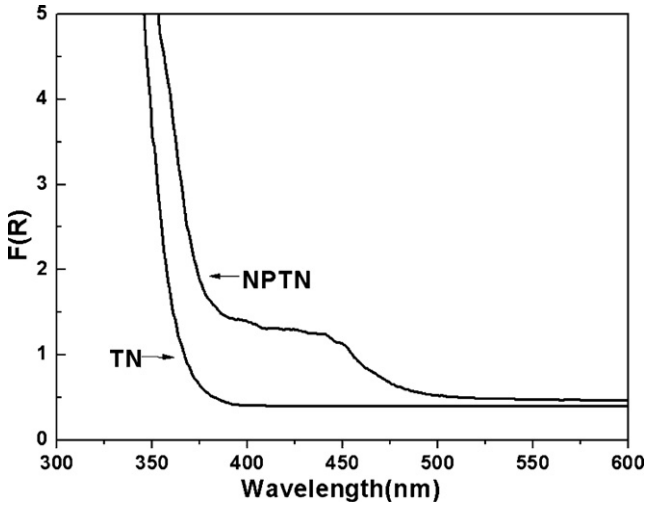

Fig. 5. UV–vis diffuse reflectance spectra plotted as K–M function $F(R)$ of TN and NPTN.

the N-doped samples should be annealed in Ar atmosphere environment.

3.3. XRD analysis

In our previous studies, the freshly prepared TiO_2 nanotube arrays is amorphous phase, and could be transformed from amorphous phase to anatase phase after being sintered at 400 °C, the rutile phase could be detected through annealing at 600 °C [4,5]. The XRD patterns of the as-prepared TiO_2 nanotube arrays are shown in Fig. 4. For the pure TiO_2 nanotube arrays sample, all the diffraction peaks can be well indexed into anatase phase, due to calcination at relative low temperature 500 °C. In comparison with the XRD patterns of TN, the diffraction peaks of rutile phase are observed in the NPTN sample, which was not observed in the pattern of TN sample, suggesting that nitrogen doping may have promoted the phase transition of TiO_2 nanotube arrays to rutile phase at low annealing temperatures [6]. The mixture phase of TiO_2 with low concentration of rutile phase is well known to show a superior potential of photocatalytic application due to mixed crystal structure [47].

3.4. UV–vis DRS analysis

Recent studies have revealed that N-doped TiO_2 nanotube arrays can lead to efficiently extending the photo response from the UV to the visible light region. Xu et al. reported that N-doped in high level TiO_2 nanotube arrays (the atomic ratio of N/Ti is 8/25) prepared by dip-calcination method showed higher visible absorbance in wavelengths regions of 400–550 nm [30]. However, even very low concentrations of nitrogen can produce considerable band gap narrowing of TiO_2 [44,45]. Liu et al. reported visible light active nitrogen doping of titania nanotube arrays (N/Ti from 0.071 to 0.082) by an electrochemical approach presented a clear red-shift in the optical response of titania nanotube array [20]. Shankar et al. studied that N-doped TiO_2 nanotube arrays with chemical composition $TiO_{2-x}N_x$, up to $x = 0.23$, fabricated by anodic oxidation in electrolyte solutions containing ammonium ions, nitrate ions and fluoride ions exhibited a significant optical absorption in the visible wavelength range from 400 to 530 nm [36]. In our case, the nitrogen concentrations of the NPTN sample is approximately 2 at.%, which is sufficient to change the absorption properties.

Fig. 5 illustrates the diffuse reflection spectra of pure TiO_2 and nitrogen doped TiO_2 nanotube arrays. The results indicated that nitrogen doped sample by N_2-plasma treatment showed a clear red-shift in the optical response of TiO_2 nanotube arrays. Currently, there are some arguments about the mechanisms of the visible light activity of N-doped TiO_2. Some researchers ascribed the visible light photocatalytic sensitization of N-doped TiO_2 to the substitutional/interstitial N atoms or NO_x impiruties [30,34]; some suggested that the enhanced visible light photocatalytic activity was due to O vacancies [31]; others concluded that O vacancies of N-doped TiO_2 could result in donor states locate below the conduction bands which induces photocatalysis under visible light [32]. Most experiments can introduce O vacancies and N species, thus it is difficult to distinguish the roles of them. Lin and co-workers calculated the optical absorption spectra of N-doped and O deficient anatase TiO_2 using spin-polarize density function-theory (DFT). The results showed that the anatase TiO_2 with different concentrations of O vacancies displayed enhanced absorption in ultraviolet regions and relative high concentrations of O vacancies TiO_2 presented strong optical absorption above 500 nm, whereas N-doped TiO_2 exhibited significant absorption in the region of 400–500 nm [48]. The results are in good agreement with reports by Ihara [32] and Qiu [49]. Therefore, the visible light photocatalytic sensitization of the NPTN samples should be ascribed to the substitution of lattice O for N species, which is in agreement with the XPS result.

As compared to the pure TiO_2 nanotube arrays, the spectrum shows the absorption edge of NPTN shift to longer wavelength after doping N. The UV–vis DRS can be employed to estimate the shift in the band gap transition of the photocatalysts. Due to the Kubelka–Munk function, the band gap energy E (eV) for each specimen can be calculated by the absorption coefficient of adsorption spectra [17]. From the data of UV–vis DRS, the band gap energy of the pure TiO_2 nanotube arrays was ~3.24 eV, which is due to the pure anatase phase of TN sample. The nitrogen doped sample had two absorption edges, which might be attributed to the formation of rutile phase and nitrogen doped TiO_2, respectively. One absorption edge corresponded to ~3.03 eV and the other induced by nitrogen doping in TiO_2 lattice in visible light region to ~2.22 eV [19]. Nitrogen doping generates the absorption edge in the visible light range, which suggests that the NPTN would present high photocatalytic activity under the visible light irradiation.

3.5. PL and TEM analysis

The PL spectra have been widely used to study the transfer behavior of the photogenerated electrons and holes in semiconductor materials, so that it can reflect the separation and recombination

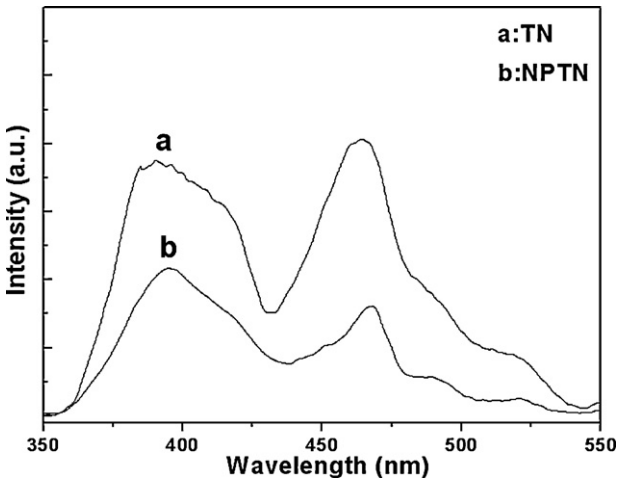

Fig. 6. PL spectra of TN and NPTN.

of photogenerated carries. Fig. 6 shows the PL spectra of the pure and N-doped TiO_2 nanotube arrays with an excitation wavelength of 300 nm. Two broad and gentle emission bands were observed in the scanning range of 350–550 nm. It is observed that the pure TiO_2 shows a broad peak in the range of 400–430 nm and an obvious peak at about 465 nm. The broad peak appeared at about 400–430 nm was ascribed to the free exciton emission and the other emission band peaked at about 465 nm was attributed to bound exciton emission, which is similar to results of the PL spectra of TiO_2 particles have also been reported by Liu et al. [17] and Ma et al. [23]. The spectra of TN and NPTN showed nearly similar curve shape except for the peak intensities. As seen from Fig. 6, the PL intensity of pure TiO_2 nanotube arrays was much higher than that of N-doped TiO_2 nanotube arrays. It is well known that the PL signals of semiconductor materials result from the recombination of photogenerated electron–hole pairs. Generally, the lower PL intensity suggested the lower the recombination rate of photogenerated electron–hole pairs, which leads to the high the photocatalytic activity of semiconductor photocatalysts [23]. Therefore, the low PL intensity for N-doped TiO_2 nanotube arrays indicates that the photocatalytic activities of TiO_2 nanotube arrays may be improved by N_2-plasma treatment.

To confirm the tubular structure and verify the crystallization of nanotubes, TEM images and HRTEM pattern were taken and the results are shown in Fig. 7. From TEM images (Fig. 7(a)), the straight hollow channel structure of the nanotubes is revealed, the thickness of the nanotubes keep almost unchanging from the top to the end. TiO_2 nanotubes obtained are uniformly distributed and have a diameter of around 140 nm with the wall thickness of 30 nm, which is in good agreement with the results obtained by FESEM measurements. Fig. 7(b) is the typical HRTEM image of a single nanotube. The clear lattice image indicates the high crystallinity of the TiO_2 nanotubes. The lattice spacing of 0.352 nm and 0.243 nm could be attributed to the (1 0 1) and (1 0 3) planes of the anatase phase. Another lattice spacing of 0.324 nm was determined corresponding to the lattice spacing of the (1 1 0) plane of the rutile phase, which is in good agreement with the XRD and PL results.

3.6. Photoelectrochemical behavior and evaluation of photocatalytic activity

The photocurrent responses of the N-doped sample and the undoped sample at the applied voltage of 0 V are shown in Fig. 8. The responses of both electrodes were prompted to visible light irradiation. Comparing with the undoped sample, the N-doped sample demonstrated superior performance with higher photocurrent generation efficiency. The photocurrent intensity of

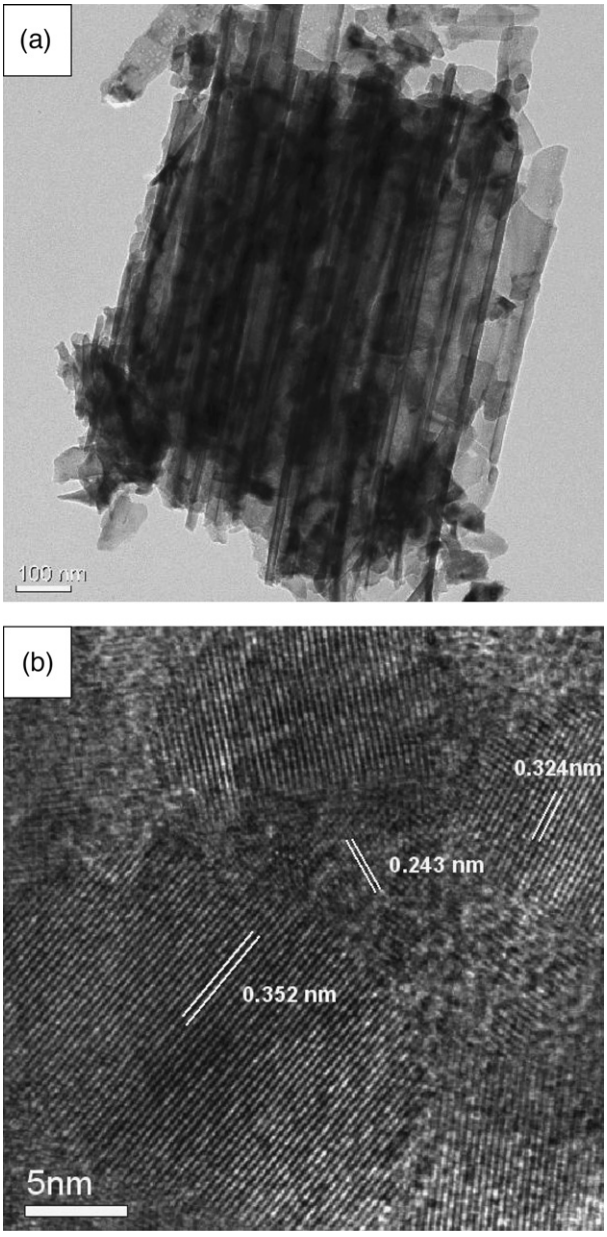

Fig. 7. TEM and HRTEM images of NPTN.

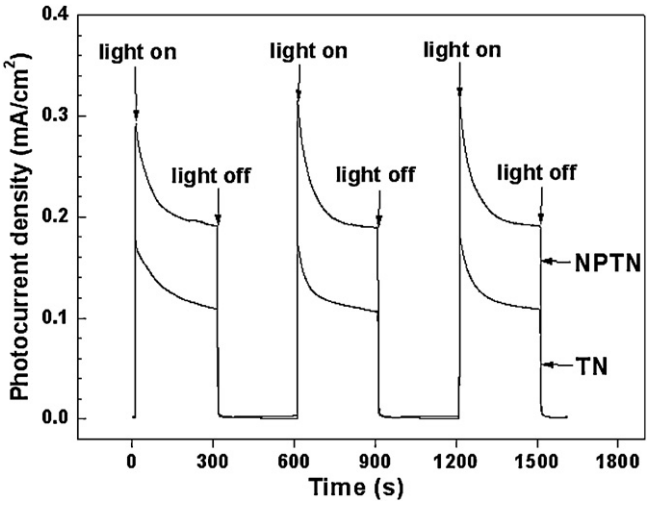

Fig. 8. Photocurrent response of TN and NPTN.

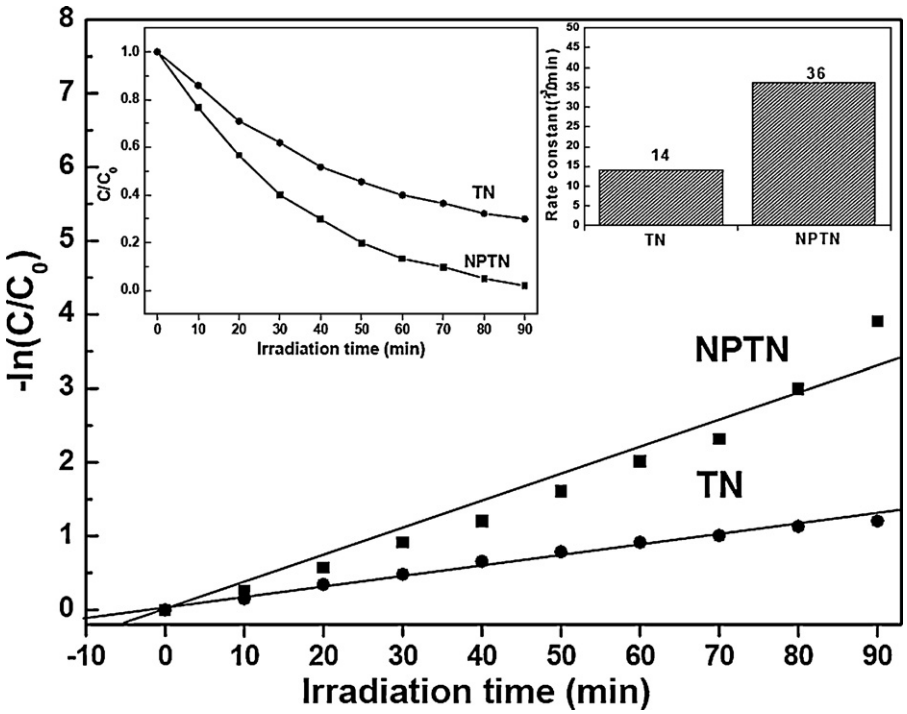

Fig. 9. Photocatalytic degradation rates of MB for TN and NPTN. Inset is kinetic of MB degradation for TN and NPTN.

the NPTN sample is 0.19 mA cm^{-2}, which is ~2 times higher than that of the TN sample (0.09 mA cm^{-2}). Higher photocurrent density suggests that the photogenerated charge carriers transfer more effectively from the working electrode to the counter electrode and greater activity in the photocatalysis process [35].

The photocatalytic activities of the NPTN and the TN samples were evaluated with the degradation of MB under the visible light irradiation, as shown in Fig. 9. The blank test without photocatalyst was also researched, but only a small amount (~3%) of MB was degraded under intensive visible light. The amount of MB decompounded by the NT sample was only 68% after 90 min of irradiation while the amount of MB decompounded by the NPNT sample was almost 98%. It is evident that the plot of $-\ln(C/C_0)$ versus irradiation time exhibits a good linear relationship. The apparent reaction rate constant k_{obs} could be calculated using pseudo-first-order pattern, based on the following equation [21,34]:

$\ln(C/C_0) = -k_{obst}$, where t is the irradiation time, C_0 is the initial concentration of MB in aqueous solution and C is the residual concentration of MB solution. The value of k_{obs} was obtained by the slope of the liner region between $-\ln(C/C_0)$ and the irradiation time (see Fig. 9). Comparing with the NT sample (0.014 min^{-1}), the NPNT sample (0.036 min^{-1}) displays a significant enhancement of photocatalytic activity under the visible light irradiation. Since the TN and NPTN samples have the similar surface morphologies, hence, doping N into TiO_2 nanotube arrays by N_2-plasma is considered to be a main factor for this improvement of photocatalytic activity. Theoretical studies have indicated that interstitial nitrogen could introduce two bonding states, which are deep in the midgap region and lie below the top of the valence band O 2p states, respectively. The bonding states in the midgap region lie above the O 2p band and are higher in the gap than the N 2p states generated by substitutional nitrogen [37]. Thus, the new energy level caused by doping of N can narrow wide band gap of TiO_2 and improve the efficiency of utilizing sunlight. Furthermore, the coexistence of anatase phase and a low content of rutile phases also can enlarge the photocatalytic activity of TiO_2 samples. Zhang and et al. [47] synthesized mixture of anatase phase and rutile TiO_2, and suggested that the mixture of anatase TiO_2 and a small amount of rutile TiO_2 presented better photocatalytic activity than the pure anatase TiO_2, due to heteojunction structure formed between interface of anatase and rutile phases, which can inhibit the recombination of photogenerated electrons and holes because of their different Fermi level. Herein, coexistence of mixture phases in NPTN is helpful for enhancing the separation between photoinduced electrons and holes. As a result, N-doping by treatment with N_2-plasma not only enlarges their absorbance band to visible light region, but also improves photocatalytic activities of TiO_2 nanotube arrays.

4. Conclusions

In summary, highly ordered and high aspect ratio TiO_2 nanotube arrays were prepared by anode oxidization method of Ti foils in the fluorine containing glycerol-base electrolyte and then treated with N_2-plasma. It is found that the incorporation of N element into the TiO_2 lattice accelerates the transformation from anatase to rutile phase at low annealing temperatures. The N-doped TiO_2 nanotube arrays exhibited considerable absorption capacity in the visible light region and great photocurrent density. MB degradation model experiments showed that the N-doped TiO_2 nanotube arrays presented a significantly enhancement of the photocatalytic activity comparing with the pure TiO_2 nanotube arrays under the visible light irradiation. Therefore, here a new pathway is provided to construct nano-structure composite materials with high photocatalytic activity in visible light region benefiting from N-doped using N_2-plasma treatment.

Acknowledgements

We are grateful to Hongge Pan for critical reading and editing of this manuscript. This work was supported by National Basic Research Program of China (973Program, 2011CB201202) of Ministry of Science and Technology of China (MOST), National Natural

Science Foundation of China (20776089 and 50774053) and the 985 Project of Sichuan University. The authors would like to express their heart-felt gratitude to Analytical and Test Center of Sichuan University and gratefully acknowledge the TEM Group of Analytical Testing Center of Sichuan University. Chaoliang Zhao, worked at the State Key Laboratory of Oral Medicine of China, was also acknowledged for his kind help in FE-SEM observations.

Appendix A. Supplementary data

Supplementary data associated with this article can be found, in the online version, at doi:10.1016/j.jallcom.2011.08.003.

References

[1] A. Fujishima, K. Honda, Nature 238 (1972) 37–39.
[2] D. Trong On, D. Desplantier-Giscard, C. Danumah, S. Kaliaguine, Appl. Catal. A 222 (2001) 299–357.
[3] J.M. Macak, M. Zlamal, J. Krysa, P. Schmuki, Small 3 (2007) 300–304.
[4] Y.L. Liao, W.X. Que, Z.H. Tang, W.J. Wang, W.H. Zhao, J. Alloys Compd. 509 (2011) 1054–1059.
[5] J. Bai, Y.B. Liu, J.H. Li, B.X. Zhou, Q. Zheng, W.M. Cai, Appl. Catal. B: Environ. 98 (2010) 154–160.
[6] Y.K. Lai, J.Y. Huang, H.F. Zhang, V.P. Subramaniam, Y.X. Tang, D.G. Gong, L. Sundar, L. Sun, Z. Chen, C.J. Lin, J. Hazard. Mater. 184 (2010) 855–863.
[7] G.K. Mor, O.K. Varghese, M. Paulose, K.G. Ong, C.A. Grimes, Thin Solid Films 496 (2006) 42–48.
[8] O.K. Varghese, D.G. Gong, M. Paulose, K.G. Ong, E.C. Dickey, C.A. Grimes, Adv. Mater. 15 (2003) 624–627.
[9] P. Zhong, W.X. Que, J. Zhang, Q.Y. Jia, W.J. Wang, Y.L. Liao, X. Hu, J. Alloys Compd. 509 (2011) 7808–7813.
[10] J.H. Bang, P.V. Kamat, Adv. Funct. Mater. 20 (2010) 1970–1976.
[11] G.K. Mor, K. Shankar, M. Paulose, O.K. Varghese, C.A. Grimes, Nano Lett. 6 (2006) 215–218.
[12] K.G. Ong, O.K. Varghese, G.K. Mor, K. Shankar, C.A. Grimes, Sol. Energy Mater. Sol. Cells 91 (2007) 250–257.
[13] G.K. Mor, K. Shankar, M. Paulose, O.K. Varghese, C.A. Grimes, Nano Lett. 5 (2005) 191–195.
[14] M. Paulose, G.K. Mor, O.K. Varghese, K. Shankar, C.A. Grimes, J. Photochem. Photobiol. A, Chem. 178 (2006) 8–15.
[15] H.J. Yan, H.X. Yang, J. Alloys Compd. 509 (2011) L26–L29.
[16] R. Asahi, T. Ohwaki, K. Aoki, Y. Taga, Science 293 (2001) 269–271.
[17] X.F. Chen, X.C. Wang, Y.D. Hou, J.H. Huang, L. Wu, X.Z. Fu, J. Catal. 255 (2008) 59–67.
[18] J.G. Yu, Q.J. Xiang, M.H. Zhou, Appl. Catal. B: Environ. 90 (2009) 595–602.
[19] J.S. Wang, Z.Z. Wang, H.Y. Li, Y.T. Cui, Y.C. Du, J. Alloys Compd. 494 (2010) 372–377.
[20] R.A. Doong, T.C. Hsieh, C.P. Huang, Sci. Total Environ. 408 (2010) 3334–3341.
[21] H. Yang, C.X. Pan, J. Alloys Compd. 501 (2010) L8–L11.
[22] Q. Ma, S.J. Liu, L.Q. Weng, Y. Liu, B. Liu, J. Alloys Compd. 501 (2010) 333–338.
[23] Y.F. Tu, S.Y. Huang, J.P. Sang, X.W. Zou, J. Alloys Compd. 482 (2009) 382–387.
[24] O. Diwald, T.L. Thompson, E.G. Goralski, S.D. Walck, J.T. Yates, J. Phys. Chem. B 108 (2004) 52–57.
[25] T. Lindgren, J.M. Mwabora, E. Avendan, J. Jonsson, A. Hoel, G. Granqvist, S. Lindquist, J. Phys. Chem. B 107 (2003) 5709–5716.
[26] Y. Wang, C.X. Feng, Z.S. Jin, J.W. Zhang, J.J. Yang, S.L. Zhang, J. Mol. Catal. A: Chem. 260 (2006) 1–3.
[27] G. Liu, F. Li, D.W. Wang, D.M. Tang, C. Liu, X.L. Ma, G.Q. Lu, H.M. Cheng, Nanotechnology 19 (2008) 025606.
[28] A. Ghicov, J.M. Macak, H. Tsuchiya, J. Kunze, V. Haeublein, S. Kleber, P. Schmuki, Chem. Phys. Lett. 419 (2006) 426–429.
[29] A. Ghicov, J.M. Macak, H. Tsuchiya, J. Kunze, V. Haeublein, L. Frey, P. Schmuki, Nano Lett. 6 (2006) 1080–1082.
[30] J.J. Xu, Y.H. Ao, M.D. Chen, D.G. Fu, Appl. Surf. Sci. 256 (2010) 4397–4401.
[31] Y. Nakano, T. Morikawa, T. Ohwaki, Y. Taga, Appl. Phys. Lett. 86 (2005) 132104.
[32] T. Ihara, M. Miyoshi, Y. Iriyama, O. Matsumoto, S. Sugihara, Appl. Catal. B: Environ. 42 (2003) 403–409.
[33] Z.Q. Liu, Y.C. Wang, W. Chu, Z.H. Li, C.C. Ge, J. Alloys Compd. 501 (2010) 54–59.
[34] J. Ananpattarachai, P. Kajitvichyanukul, S. Seraphin, J. Hazard. Mater. 168 (2009) 253–261.
[35] H.J. Liu, G.G. Liu, X.Y. Shi, Colloid Surf. A 363 (2010) 35–40.
[36] K. Shankar, K.C. Tep, G.K. Mor, C.A. Grimes, J. Phys. D: Appl. Phys. 39 (2006) 2361–2366.
[37] C.D. Valentin, G. Pacchioni, A. Selloni, S. Livraghi, E. Giamello, J. Phys. Chem. B 109 (2005) 11414–11419.
[38] D. Fang, K.L. Huang, S.Q. Liu, Z.P. Luo, X.X. Qing, Q.G. Zhang, J. Alloys Compd. 498 (2010) 37–41.
[39] D.R. Baker, P.V. Kamat, Adv. Funct. Mater. 19 (2009) 805–811.
[40] Q. Zheng, H. Kang, J.J. Yun, J.Y. Lee, J.H. Park, S. Baik, ACS Nano 5 (2011) 5088–5093.
[41] F. Chen, Z.G. Deng, X.P. Li, J.L. Zhang, J.C. Zhao, Chem. Phys. Lett. 415 (2005) 85–88.
[42] L.X. Yang, D.M. He, Q.Y. Cai, C.A. Grimes, J. Phys. Chem. C 111 (2007) 8214–8217.
[43] J.M. Macak, F. Schmidt-Stein, P. Schmuki, Electrochem. Commun. 9 (2007) 1783–1787.
[44] C.M. Teh, A.R. Mohamed, J. Alloys Compd. 509 (2011) 1648–1660.
[45] S. Rani, S.C. Roy, M. Paulose, O.K. Varghese, G.K. Mor, S. Kim, S. Yoriya, T.J. LaTempa, C.A. Grimes, Phys. Chem. Chem. Phys. 12 (2010) 2780–2800.
[46] J. Lin, J.F. Chen, X.F. Chen, Electrochem. Commun. 12 (2010) 1062–1065.
[47] J. Zhang, Q. Xu, Z. Feng, M. Li, C. Li, Angew. Chem. Int. Ed. 47 (2008) 1766–1769.
[48] Z.S. Lin, A. Orlov, R.M. Lambert, M.C. Payne, J. Phys. Chem. B 109 (2005) 20948–20952.
[49] X.F. Qiu, Y.X. Zhao, C. Burda, Adv. Mater. 19 (2007) 3995–3999.